Thermo magnetic {FEM} simulation of a {PM} synchronous motor with input data from telemetry driving cycles

Thermo magnetic FEM simulation of a PM synchronous motor with input data from telemetry driving cycles

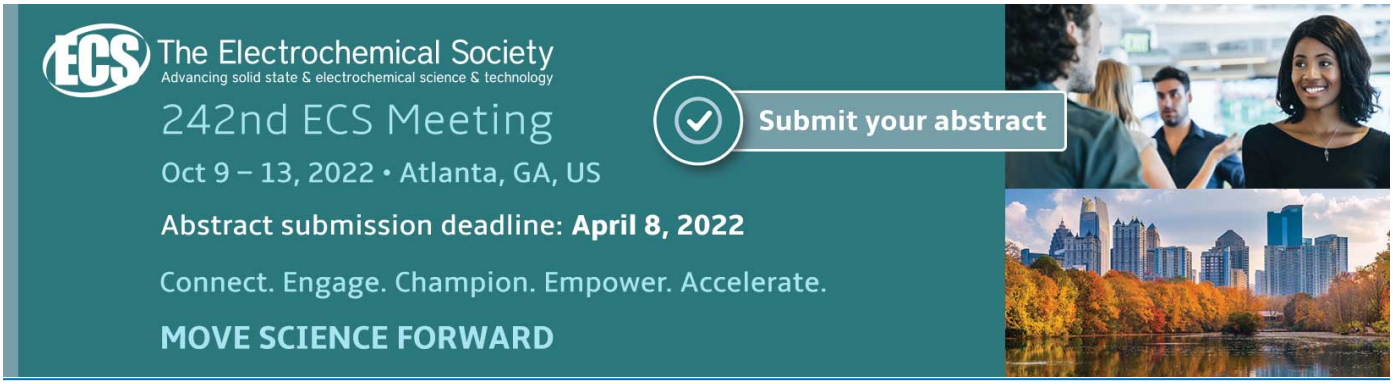

Thermo magnetic FEM simulation of a PM synchronous motor with input data from telemetry driving cycles

A Somà, F Mocera and S Venuti

Politecnico di Torino, Department of Mechanical and Aereospace Engineering, Corso Duca degli Abruzzi 24, 10129 Torino, Italy

E-mail: aurelio.soma@polito.it

Abstract. Nowadays, the requirements to reduce greenhouse gas emissions and to provide a healthy and more habitable environment, has led to the development of several sustainable alternative for eco-mobility. Since the improvement of internal combustion engine has reached a steady state point in terms of overall efficiency, the increasingly stringent requirements imposed by international normative standards are leading automotive companies to find other alternatives to reduce pollution. Thanks to the exponentially growth of power electronics, the huge interest on research of high energy and power density batteries and the more integration of the embedded systems, the central role of the electric drive has taken over on most of vehicles applications. The wide use of permanent magnets synchronous motors for electric vehicles application has rapidly spread out, thanks to their capability to provide high torque and efficiency with low weight and size. Since the natural behaviour of permanent magnets to demagnetize under severe conditions, both coupled thermal and magnetics, the necessity to understand and predict the phenomena is mandatory. This paper carries out a performance analysis in duty cycle, given by real CAN and GPS readings in a studied pathway, with discussion of numerical and graphic technical evaluations. Finite element software has also been used for coupled electromagnetic and thermal calculation to set the magnets working point and establish the temperature distribution within the motor itself during the whole thermal transient. A particular overview is done on the dependence of material used and different cooling solutions adopted.

1. Introduction

Earth's changing climate has several impacts on individual mobility[1], logistics and agriculture[2]. In the last years many companies have been announcing their conversion to produce only zero-emission vehicles. This strong shift has been made possible thanks to the consumer sentiment, buffered also by the extended financial incentives, the growth in charging infrastructures and the expansion on the affordable models available. With the recent progress in the power electronics control[3], AC motors are suppressing almost all the applications in which electric motors are involved. Research in magnetic materials has led to the use of rare-earth magnets that enhances the motor power, but at the same time they are more prone to demagnetize under thermal stress[4]. To develop more power, a strong attention needs to be paid on how batteries[5] fed the motor and on their energy capacity and current discharge rate which enhance the peak torque achievable, taking into account also the inherent stress[6] along the charge and discharge cycle. In the context of the Industry 4.0, which has been representing the fourth industrial revolution, refers to the continuous communication between machines and network to prevents faults, programming maintenance and allowing real time remote control. To integrate all components constituting this chain, it is essential the development of a platform in which all the

information are collected, so the role of big data management and the IoT become crucial. Furthermore, once these data are stored, simulation covers a central role in solving problems or accurately predict the maintenance needed. This paper carries out a performance analysis of a full electric vehicle test bench using an Arduino based electronic platform as acquisition system[7]. To accomplish this goal, starting from the mechanical characteristics declared by the manufacturer, a permanent magnet synchronous motor (shortened PMSM) was designed following a reverse engineering procedure. Furthermore, data acquired by the electronic platform are collected and filtered, separating the ones referring to the vehicle from the motor ones. So, resorting to coupled GPS and data visualization the correct functioning of the motor is examined. If particular functioning conditions are observed, these data become the input for the duty cycle FEM simulation in Ansys MotorCad with the previously designed motor. The investigation aims to control thermal and magnetic behavior avoiding demagnetization fault, which determines costs related to magnets substitution and to machine down-time. Finally, the calculation of a simple performance index is proposed with the aim of describing how far magnets are from their critical condition and if heat is properly managed.

2. Coupled electromagnetic model

The electric motor investigated in this work is a PMSM which characteristics to be replicated are:

Table 1. Manufacturer's technical specifications.

	Value	Unit
N. Pole	6	-
n_{nom}	9000	rpm
P_{nom}	43	kW
C_{nom}	45	Nm
BEMF	180	V_{RMS}
I_{nom}	150	A_{RMS}

Dealing with electric motors the design consists of a fixed stator and a rotating rotor, held in place by the use of bearings and separated by a thin layer of air called air-gap.

First the stator design is carried out by considering an integral slot motor, in a way in which the harmonics produced by each winding are in phase with each other, so the total number of slots is found considering one coil per pole per phase. Choosing a number of magnet poles N_m=6 and by considering a three phase alternating currents, the number of slots constituting the stator lamination N_s=18 was calculated. Therefore, the value of air gap length comes out from a tradeoff between the cogging torque and torque produced. A good compromise is obtained with[8] :

$$g=\frac{N_s}{2\,N_m} \tag{1}$$

Where g is the amount of stator yoke required for each magnet pole.

Considering a commercially available magnet length of 40 mm, the magnetic flux density in the air gap is determined by the magnets thickness, an increase in this dimension reduces the motor inductance. A desired condition is a higher inductance coupled to a high flux density. From the simulations, to match motor specifications, magnets need to be 4 mm thick with an arc length of 150 °Electrical. The overall dimensions of the motor designed are:

Table 2. Geometry properties of the designed motor.

Data	Value (mm)
Φ_{ext}	220
Φ_{bore}	126
Airgap	1.5
Φ_{shaft}	40

Where drawing dimensions are shown in figure 1 and figure 2.

To complete the stator design a supposed lamination material has been chosen by considering its magnetics properties. Thus, was calculated dimensions of stator teeth and radial back iron length. In addition, since the space are constrained by the destination place, knowing relation of the torque:

$$T=kD^2L \tag{2}$$

length is consequently adjusted to fit the requirement, obtaining a motor with 3 axial slice of magnets covering a length of 120 mm while the overall motor length reach 280 mm considering the space in which are placed windings overhang. Since all these aforementioned data are hypothesis based on simulations output, it is necessary to consider an uncertainty on the data so as the material achieved. To conclude this treatment about the electromagnetic design, reducing the torque ripple[9] involves a shifting of a row from each other by an angle determined from the following relations:

$$\alpha_{skew}=\frac{N_m}{N_s}\cdot 180=60°E \tag{3}$$

Since the correspondence between electrical degree and mechanical degree is:

$$\theta_M=\theta_E\cdot\frac{2}{N_m} \tag{4}$$

Where N_m is the number of magnetic poles, the skewing angle in mechanical degree is found considering also the number of magnetic rows:

$$\alpha_{skew_M}=\alpha_{skew_E}\cdot\frac{2}{N_m}\cdot\frac{1}{N_{rows}}=6.67°M \tag{5}$$

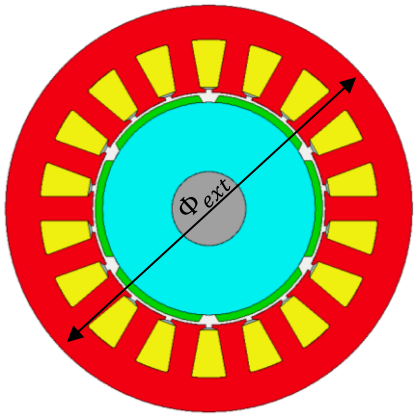

Figure 1. Radial section of PMSM designed

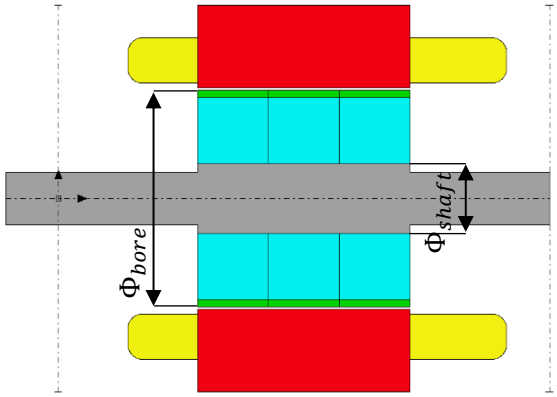

Figure 2. Axial section of the PMSM designed.

2.1. Electromagnetic analysis of motor

Before reaching the final configuration, many attempts were done maintaining as constants internal geometric data, because other parameters could determine the performance of the machine in terms of power and voltage, such lamination material, thickness, winding configuration, ferromagnetic material and temperature conditions. Temperature takes effect on the flux density remanence B_r. In fact, when increasing T, B_r decreases becoming zero at Curie's temperature. The following simulations are conducted with an internal temperature of 80°C at which the motor withstand after a starting transient.

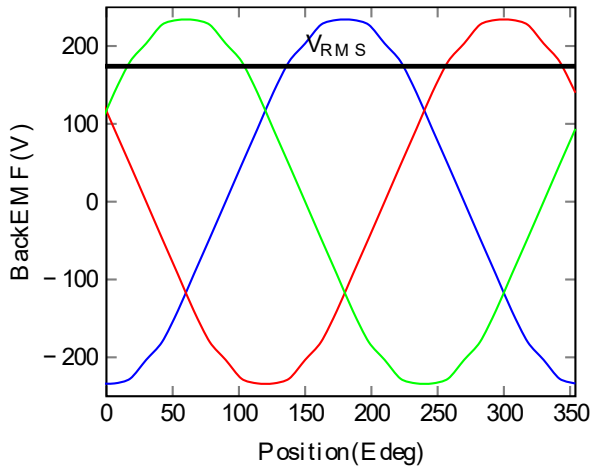

Figure 3. Back electromotive force produced by the motor

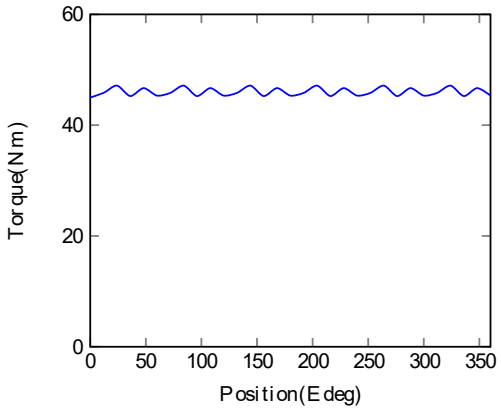

Figure 4. Total torque developed from each slice contribution

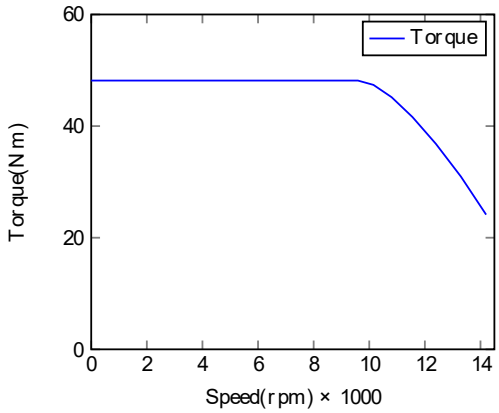

Figure 5. Torque envelope as function of the speed

All the relevant parameters are in line with the specifications and the cogging torque is arranged on 4% thanks to the magnets skewing. The efficiency obtained at nominal point working condition is η=96% using the following configuration of winding:

Table 3. Winding definition

	Value	Unit
N. Turns	2	-
Layers	2	-
N. Strands	70	-
Cond/slot	280	-
Φ_{wire}	0.885-0.8	mm

3. Electronic acquisition system to telemetry monitoring

With the spread of Industry 4.0, necessity in systems remote monitoring through telemetry platforms becomes important, in order to reduce machine downtime and to predict failure, in the view of a continuous improvement in the design of projects. In this paper the electronic system used is based on Arduino components and consists of:

- Arduino Mega
- Can Bus shield
- IMU 9-axis motion sensor
- GPS shield

The boards are used to read vehicle information available on the CAN-Bus communication line and to save hexadecimal data on a μSD card for offline post processing. The inertial measurement unit, with a data fusion algorithm, couples accelerometer, gyroscope and magnetometer readings, making available linear and gravity acceleration on each axis composing the 3-axis frame. Moreover, the gyroscope measures the angular velocity about the Euler's angle. Finally, to make significant the data acquired, is useful to link them with GPS coordinates, in a way to justify or make further investigations on particular vehicle behaviours.

This box is mounted on board of a “Fiat Panda” electric prototype which is propelled by the motor above described. This is a test bench allowing the study and the optimization of design control strategies. Concerning the vehicle, its overall specifications are reported in the following table:

Table 4. Vehicle specifications

	Value	Unit
Power	43	kW
Battery capacity	16	kWh
Nominal Voltage	640	V
Max speed	120	km/h
Average range	150	km

The acquisition platform is mounted on the vehicle, by connecting it to the CAN-Bus line and 12V power system. The cycle covered is stored and data are post processed with Matlab, where data are converted from hexadecimal to decimal values, a proper scaling factor and offsets are applied to make them meaningful. Finally, data are plotted to visualize information and catching functional anomalies or relevant working conditions.

3.1. Duty cycle definition

The working cycle[10] studied consists in a mixed route path, to test the vehicle in different conditions: urban, highway and uphill. To better understand the covered path a map showing the geographic data like altitude, latitude and longitude is shown in Figure 6:

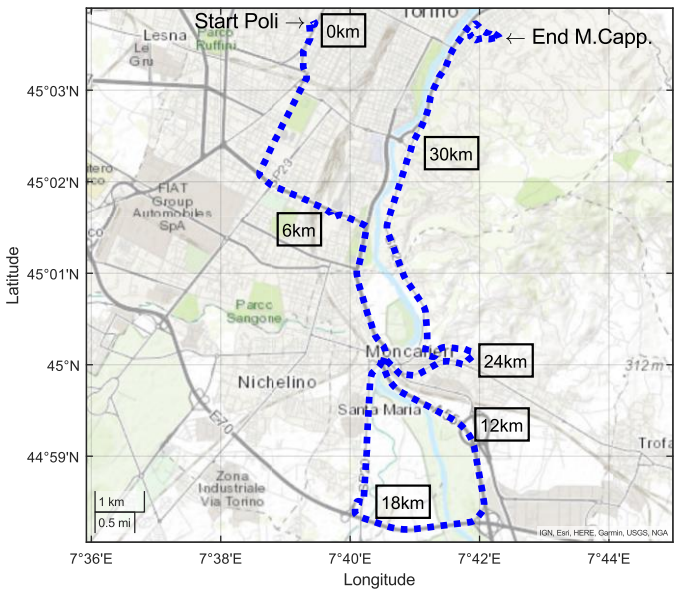

Figure 6. Driving cycle GPS path.

GPS readings report the following altitude path:

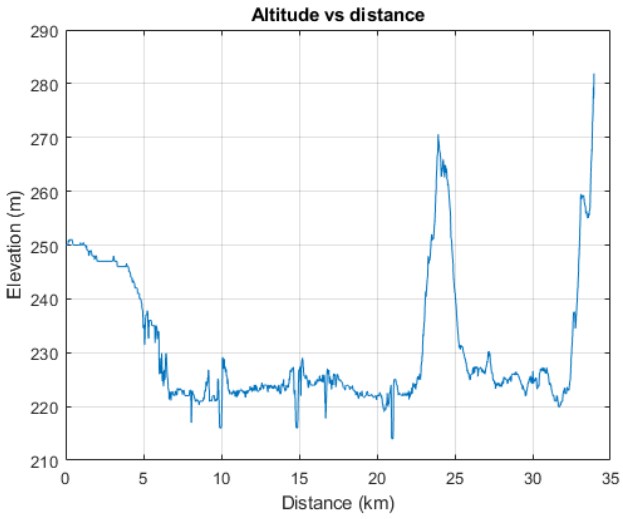

Figure 7. Altitude vs distance recorded path profile

A first skim may be sufficient to produce thoughts on power consumption and recovered energy: in particular are expected two regeneration periods coupled with two peak-power demands. The main characteristics of the covered cycle are shown below:

Table 5. Duty cycle characteristics

	Value	Unit
Space covered	34	km
Altitude difference	60	m
Average speed	36	km/h
Cycle time	60	min

By analyzing the data acquired a practical visualization on the above predicted data has been considered interesting. The following picture shows the motor power with color shades on which is superimposed the road slope represented by the markers area, in a way to analyze how the energy is used and evaluating also if the control strategy (speed or torque control based) is optimal for the prototype application.

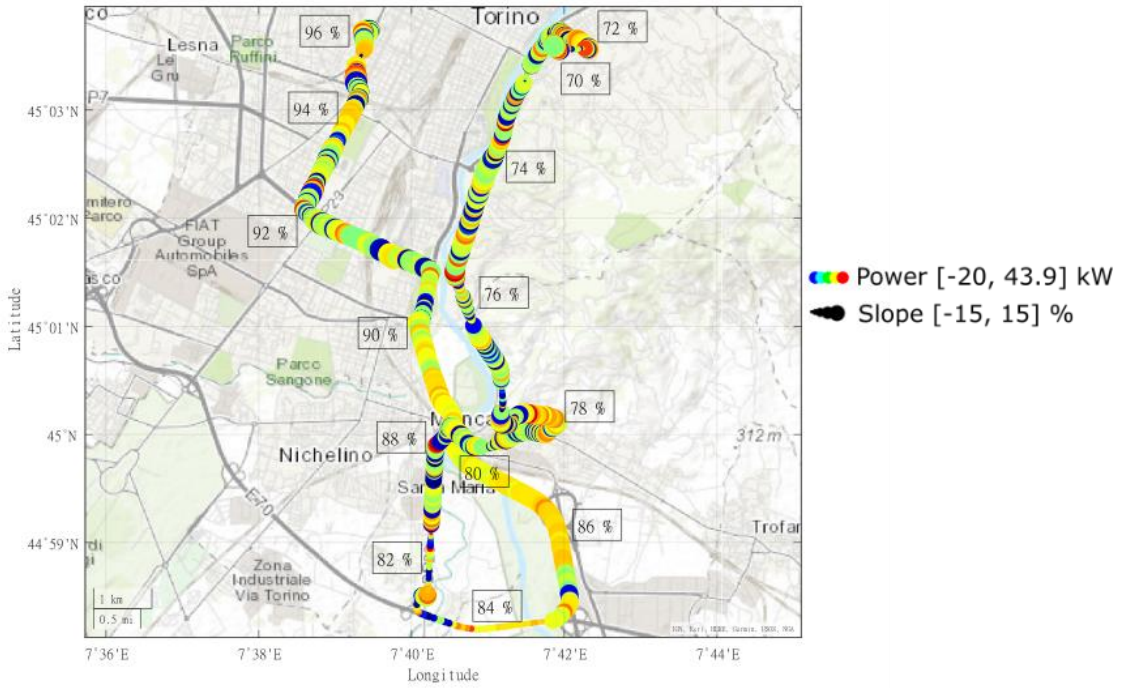

Figure 8. Power and road slope superimposed path with reference to battery SOC (%)

The above figure shows the power delivered to the motor and recovered[11], linked with altitude information and the battery-pack state of charge. To obtain a visualizable graphic GPS-altitude data are not used. Instead, a better information that describes the road slope can be given by the magnetometer readings. Acquiring the two components of the gravity acceleration we can trace the slope, furthermore since these data are so noisy, it was necessary to apply filters making smoother the data. This plot may confirm the above stated hypothesis, if the energy recovered is in correspondence of a downhill either near continuous starts and stops due to a traffic lights. In particular, knowing the covered space from the previous picture (figure 6) we can calculate the energy consumption as:

$$Energy = \Delta SOC \cdot BatteryCapacity = 26\% \cdot 16\ kWh = 4.16\ kWh \quad (6)$$

Allowing the calculation of the battery life in terms of average space coverable, which result is reported in table 4. To understand the correct functioning of the motor, the focus is now moved to data acquired and post-processed in Matlab. First is useful to have a look to the motor characteristics data like currents, temperature and speed:

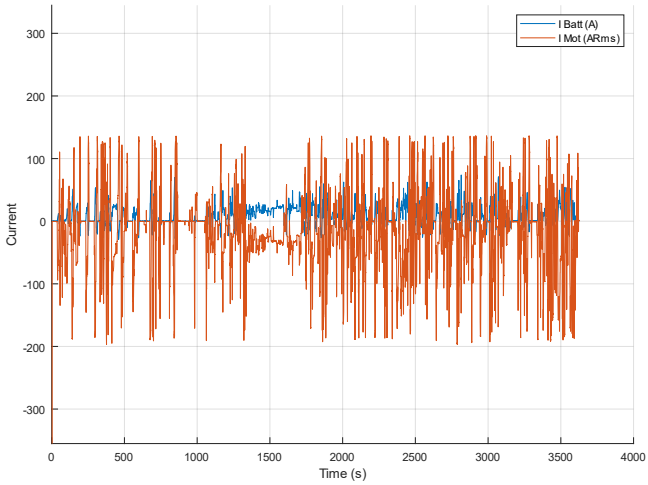

Figure 9. Motor and battery currents plot.

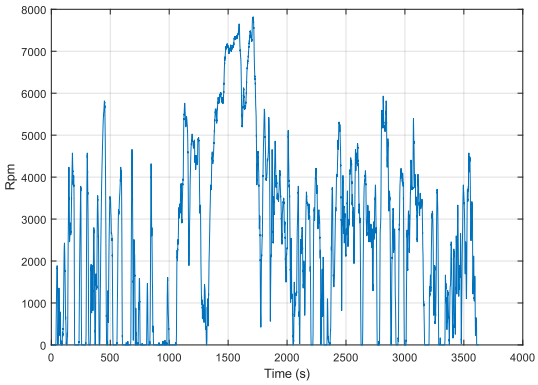

Figure 10. Motor shaft speed.

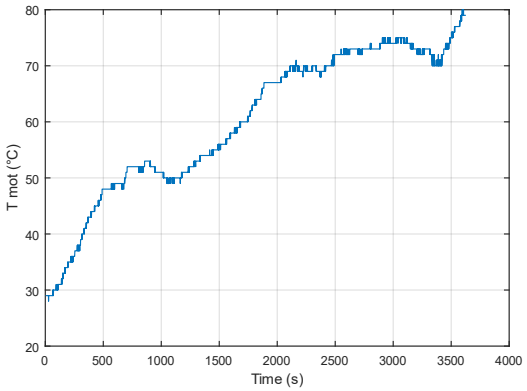

Figure 11. Temperature profile with time.

Looking at the above graphs, reported in order of visualization: in the first are plotted motor and battery currents, with opposite signs by convention: assuming positive value when battery current flows to the motor, negative value for the motor current when it receive the battery one. When torque is requested by the driver, the power electronics loops a certain amount of current to the motor, which is function of the speed. Since motor produces back electromotive force (BEMF) working against the applied voltage, the current flowing through the winding is:

$$I_{mot}=\frac{V_{drive}\text{-}BEMF}{R_{winding}} \tag{7}$$

This means that a rise in motor speed makes I_{motor} closer to $I_{battery}$, as it can be seen in the middle period (highway path) where figure 10 reports high value of motor speed. In addition, a further evaluation regards the temperature, the figure 11 shows a continuously rising suggests that no thermal equilibrium occurs within the motor and that thermal management deserves a review. Back to the figure 9, it can show motor health in the sense that if demagnetization takes place, due to thermal either uncontrolled

magnetic field produced by extremely high currents, motor loose its capacity in BEMF production, so contrary to as we used to see before, at high speed motor current doesn't get closer to battery current.

3.2. MotorCad FEM simulation

To understand possible faults or to simulate effects of a thermal design review Ansys MotorCad is used, a FEM-based software which allows to evaluate design improvements effects on the reviewed motor project. From the design discussed in Section 2, acquired data have been used to visualize motor performance. Data input of the model are the motor currents and speed as a function of time and the outputs are all motor data at each step with corresponding losses, used then as thermal simulation input.

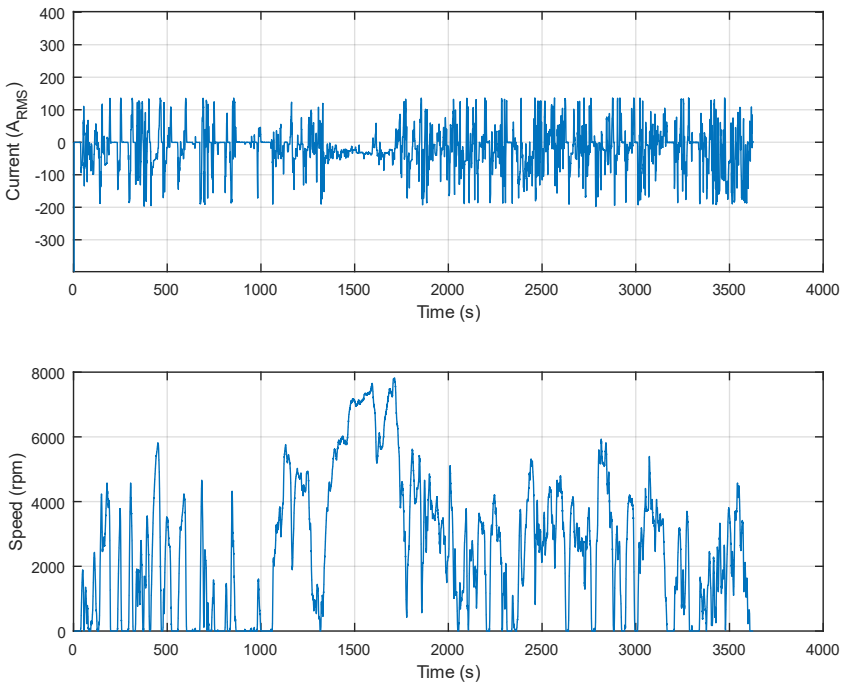

Figure 12. Motor current and motor shaft speed for MotorCad duty cycle simulations.

These data allow for calculation of point to point performance. From the calculated shaft power and knowing battery output power it is possible to estimate the overall efficiency:

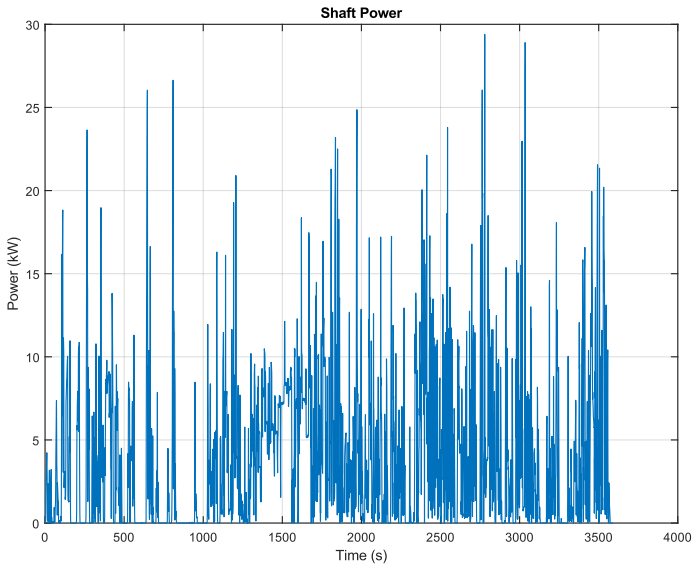

Figure 13. Shaft output motor power calculated with MotorCad simulation.

The overall efficiency calculated as product of $\eta_g=\eta_{electronics}\cdot\eta_{motor}=70\%$ where the electronics efficiency includes all the power thermal losses (wires, EPM, inverter). A similar result can be found using manufacturer's K_t to find torque, so using speed to calculate shaft power. In the following table are reported data that describes the complete cycle of the motor:

Table 6. Output duty cycle simulation

	Value	Unit
Average efficiency	88.6	%
Electrical input energy	3250	Wh
Shaft motoring energy	3100	Wh
Recovered energy	695	Wh
Shaft-generated energy	730	Wh
Total loss	190	Wh
% Motor	75.7	%
% Generator	25.3	%

Visualizing all the working points on the efficiency map of the designed motor, considerations about the motor size and the proper design for the application can be made.

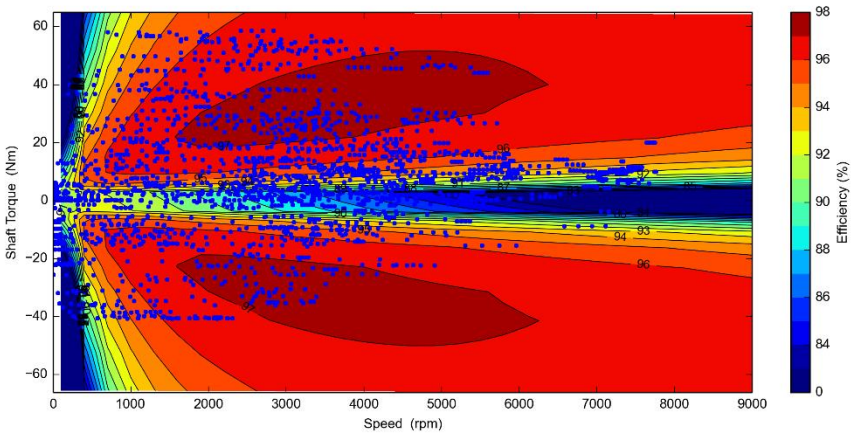

Figure 14. Motor efficiency map with duty cycle working points.

As can be seen just a little amount of the total points are in the high efficiency region as the combination of torque and speed. The other part are in a lower efficiency area, this is the reason of the average efficiency reported in table 6. Most of the working points are settled in the low efficiency region of the map, with a combination of low torque and high speed, this suggests that a further review should move points through high efficiency improving losses and energy consumption, this could be made by use of a different control strategy like a variable phase angle instead a constant one fixed to zero.

3.3. MotorCad thermal review simulation

The advantage of this software is the easy way with which multiphysics simulations are made, by passing from mechanical to thermal one and evaluating the effect of their mutual interaction. Losses calculated in the duty cycle simulation are used as inputs for the thermal model.

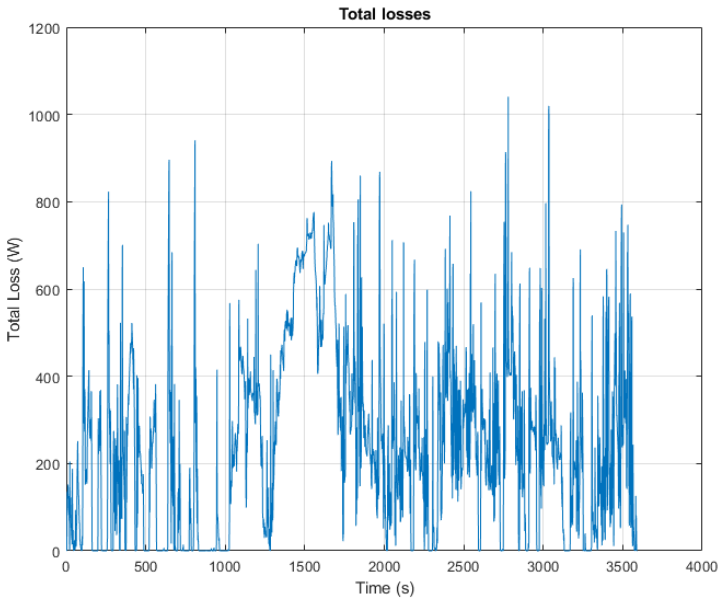

Figure 15. Motor losses calculated.

As stated from the Steinmetz's equation losses depend on the current frequency:

$$P_w=k\cdot f^a B^b \quad (8)$$

Where k,a,b are the Steinmetz's coefficients depending on interpolation from material B-H curve and the calculated P_w is expressed as power per unit of mass $\frac{w}{kg}$. Concerning material[12], the requests are high magnetic flux permeability and low losses. Since the power losses are proportional to $P_w=RI^2$ the lower is the current, the lower will be losses. So, to reduce eddy currents in the laminations electrical steel is widely used, in which the presence of silicon increases resistivity reducing the current produced, following the Ohm's law $I=\frac{V}{R}$. In this work, M350-50A electrical steel is used for stator and rotor laminations. The cooling system is assigned to housing water jacket with spiral ducts in which passes a cooling fluid consists in a mixture of water and ethylene glycol 50/50, chosen thanks to their good capability in heat absorption, furthermore presence of glycol rises the boiling temperature and decreases the freezing point. A first analysis consists in the evaluation of a general scenario at the end of the driving cycle, by knowing the point in which is installed the single NTC thermistor critical issues are investigated.

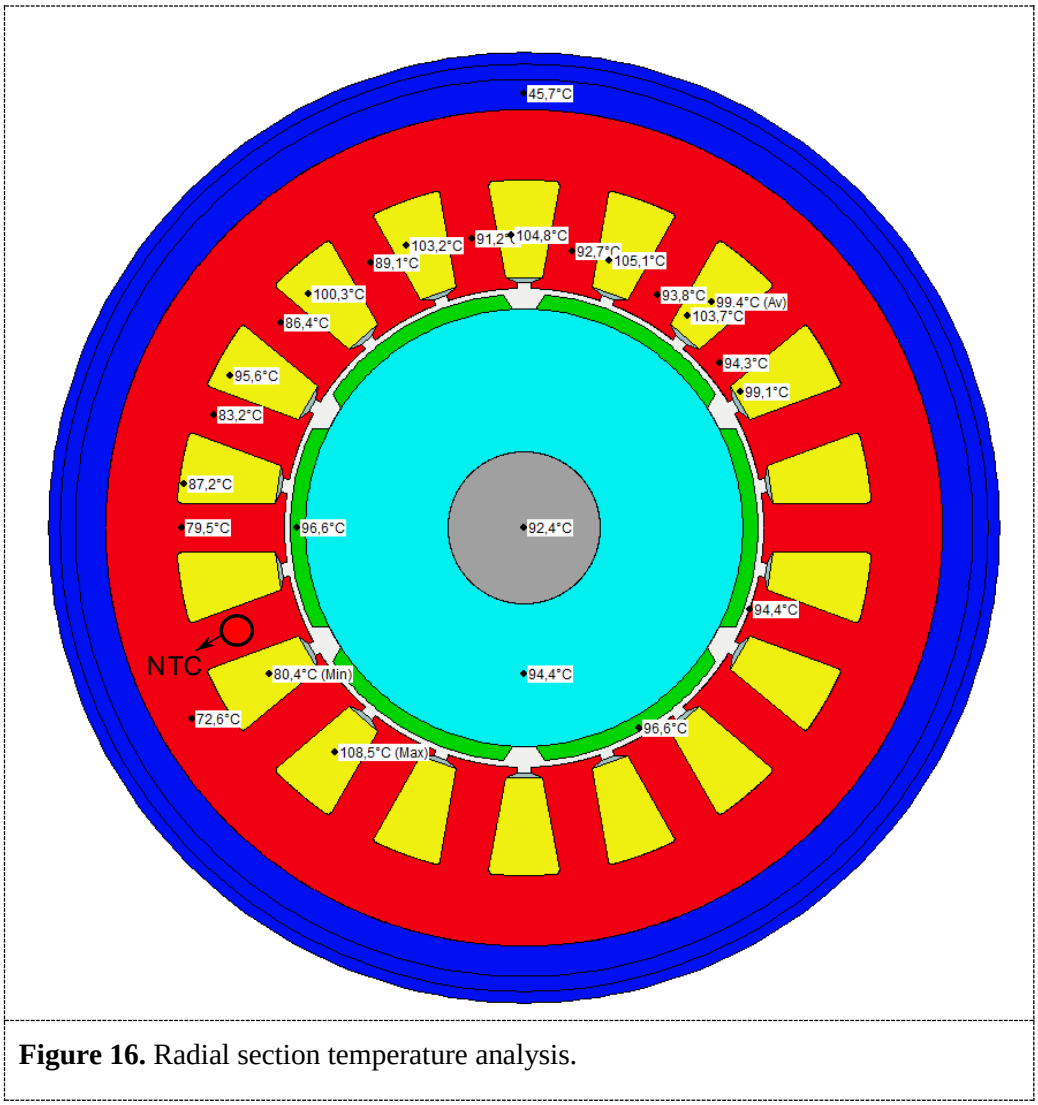

Figure 16. Radial section temperature analysis.

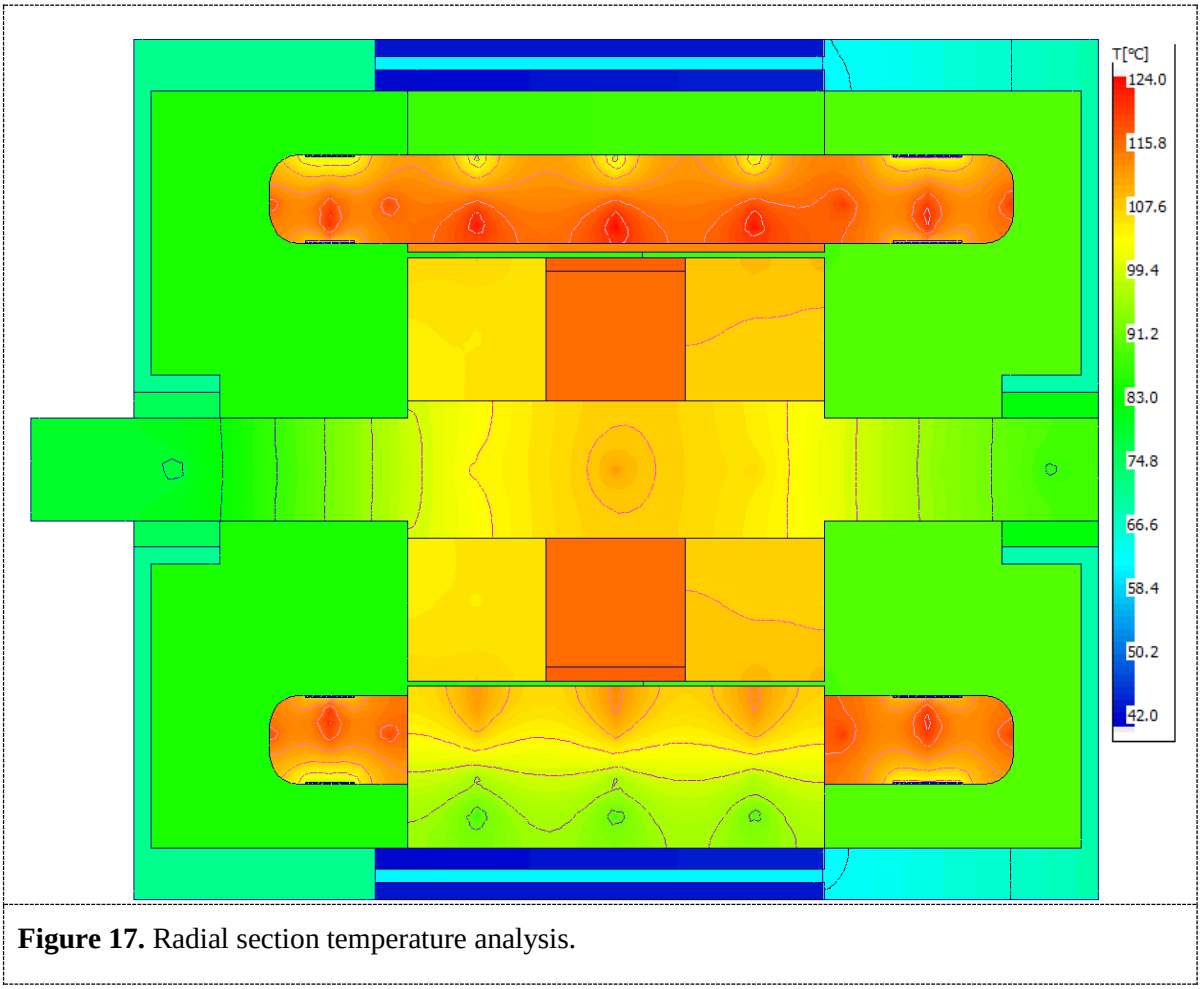

Figure 17. Radial section temperature analysis.

As it can be observed, even if we register temperature of 80°C on the external ring of the stator, in contact with cool water, internal temperature can be higher also of 20°C as the figure 14 shows. Another proof that the sensor is not well positioned is in the right figure, in which the central slice of magnets is hotter than the sides, due to the fact that exchange continuously heat with air in the endcaps region. There is an appreciable temperature difference from a side slice to a central one, of about 10°C. Generally speaking, with the used magnets N30UH 180°C class, these temperatures are not a problem, but if the using time is increased, either the power demand changes, the situation could be different. So, a general trend is to reach a steady state condition, where all the heat generated can be totally transferred to the fluid. This desired condition is achieved with a re-designed[13] cooling solution, looking for a fluid speed allows a turbulent flow and ensure high values of convective heat transfer coefficient h in the cooled region. First aluminium alloy for the inner chamber of the ducts is used, then reducing height of the channel ensures an increase in flow speed and increases structural resistance. Also the space between ducts is slightly increased, in this way endcap length can be reduced so as distance from the channel to the external surface of the stator lamination avoiding structural damage. The final geometrical configuration is:

Table 7. Radial and axial water jacket dimensions

	Value	Unit
WJ channel-lam	5	mm
WJ channel height	4	mm
WJ channel width	33	mm
WJ channel spacing	25	mm

The result achieved is an increased heat exchange surface, with enhanced heat exchange which, after a first transient, allows thermal equilibrium. As the following transient simulation[14] shows.

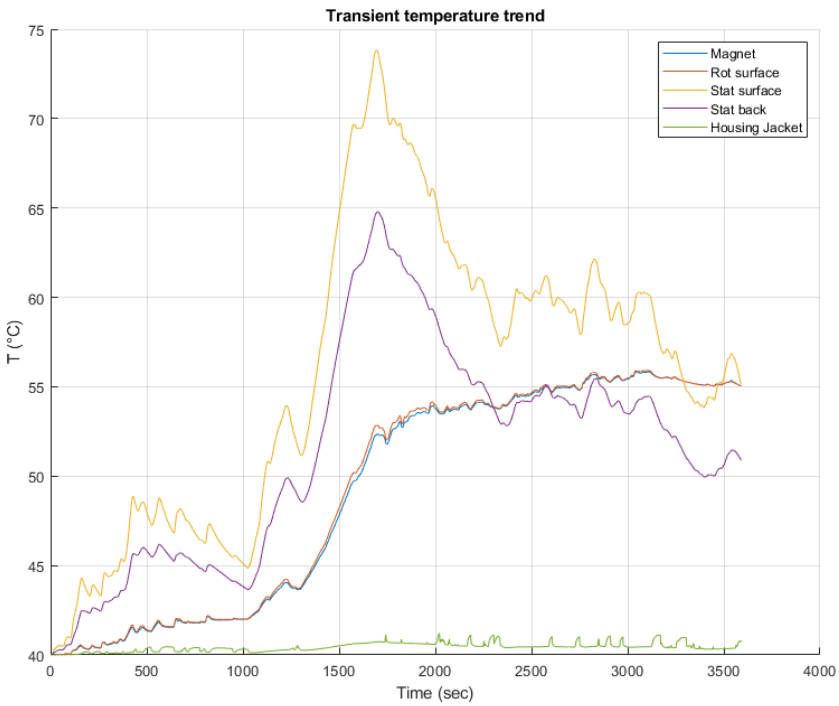

Figure 18. Duty cycle thermal analysis with reviewed cooling design

4. Demagnetization analysis[15]

Sintered NdFeB magnets are subjected to irreversible demagnetization starting from temperature of 120°C, many causes can lead to this fault: i.e. short circuits or wrong thermal management. In this section the worse condition verified in the previous duty cycle is analysed finding a safety coefficient to evaluate how far the magnets are from fault condition. When a magnet is subjected to an external

magnetic field, its behaviour is dictated by the hysteresis cycle and its working point moves along a curve called recoil line[16] parametrized with the temperature. In correspondence of the maximum temperature (for N30UH 180°C), the lines show a knee at which irreversible demagnetization occurs. Instead for temperatures lower than maximum the knee is located to negative values both of B and H. The phenomenon takes place in a sense that the remaining value of magnetic field density B_r is reduced to a value in which the magnet is not able anymore to produce BEMF. Demagnetization[17] may occurs with a coupled effect of impulsive currents and high temperature, considering that heat is generated in part in the coils and another part in laminations due to eddy current losses, cooling these hot spots represents the highest priority in thermal management. In this work is discussed a fault analysis starting from a critical point identified in the cycle. In this case, a critical point is found with the following data:

Table 8. Characteristics of critical working point

	Value	Unit
n	2090	rpm
Torque	58.7	Nm
I_{peak}	274.3	A
Power	25	kW
Temp	70	°C
Loss	635	W

In order to find a simple and representative value that defines how far is the worst condition at which magnets need to withstand. The operating point is simulated coupling electromagnetic and thermal FEM, taking into account the working temperature. With the resulting B and H it is calculated the permeance coefficient P_c defined as:

$$P_c = -\frac{B_m}{\mu_0 H_m} \tag{9}$$

Table 9. Magnetic results at critical working point

	Value	Unit
B	0.498	T
H	441.7	kA/m
P_c	0.9	-

Demagnetization curve, at working temperature of this condition shows a H_{knee}=1430 $\frac{kA}{m}$, defining the starting point of irreversible demagnetization.

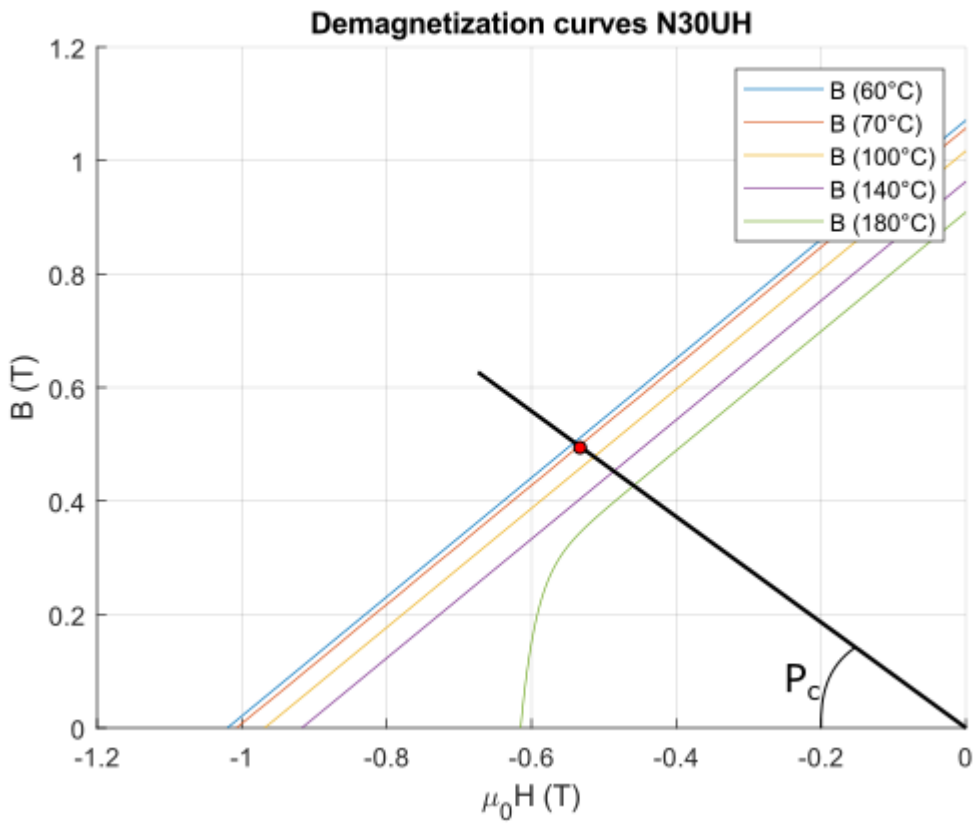

Figure 19. Demagnetization curves of magnet N30UH.

As it can been appreciated this kind of load in terms of current and heat is not critical. Instead moving to the 180°C characteristic, considering these electromagnetic conditions, since the permeance line crosses the knee point, the magnet would results more prone to demagnetize. However, the safety coefficient which represents qualitatively the distance from fault is:

$$Sf=\frac{H}{H_{knee}}=3.2 \quad (10)$$

This safety factor suggests electric motor works in a safe condition in the most loaded point of the cycle.

5. Conclusion

This work points out a method for continuous monitoring of a full electric vehicle equipped with a permanent magnets synchronous motor, by acquiring data with an electronic Arduino based system connected to the vehicle CAN-bus and by using them as input data for a reverse engineer motor from manufacturer's overall characteristics. Data have shown an unbalanced thermal management and the paper propose a re-designed cooling jacket which improve heat exchange. Furthermore, a method to analyse potentially critical working point and evaluating possible faults has been developed. Thermo-magnetic coupled FEM simulations have made it possible to detect eventual failures and calculate a value which states distance from fault. In this work the existence of a rotor retaining sleeve structure, useful to withstand the high centrifugal forces generated when the motor turns at high speed, was neglected. The high number of degrees of freedom available at the design stage of electric motor has made difficult the preliminary design, for this reason it has been necessary the use of mathematical

proportionality equations[8]. This work has pointed out the importance on the right choose of materials, in fact, many attempts to reach an acceptable efficiency have been made. The final configuration reports a higher efficiency than manufacturers specifications, considering however that the purpose of this study was matching performance neglecting costs. The analysis have shown a motor particularly responsive to heat with sudden rises in temperature recorded with the electronic tool, which behaviour was considered dependent on a underestimation of heat exchange characteristic parameters, so it was considered useful the proposal of improvements to be taken into account in the subsequent models. Finally, the last evaluation was done on demagnetization, without observing any critical scenario, that could have been occurred if the critical point would have happened at higher temperatures.
The future research will focus on more innovative cooling solutions regarding also the rotor and find materials with minor losses in a way to expand the high efficiency working range.
Further improvement may regard the implementation of a simile technique as a standard analysis for IoT remote control, allowing fault prediction or to help the service in detection of electric vehicle overall failures.

References

[1] Mocera F and Somà A 2021 A Review of Hybrid Electric Architectures in Construction, Handling and Agriculture Machines *New Perspectives on Electric Vehicles* ed Prof Marian Găiceanu (Intechopen*)*
[2] Mocera F and Somà A 2020 Analysis of a Parallel Hybrid Electric Tractor for Agricultural Applications *Energies* **13**(12) 3055
[3] B K Bose 2009 Power Electronics and Motor Drives Recent Progress and Perspective *IEEE Transactions on Industrial Electronics* **56**(2) pp 581-588
[4] Tae-Kyoung B, Kyung-Hun S, Jeong-In L, Jong-Hyeon W, Han-Wook C and Jang-Young C 2021 Design of high-speed permanent magnet synchronous machines considering thermal demagnetization and mechanical characteristic of permanent magnet *AIP Advances* **11** 025129
[5] Mocera F, Vergori E and Somà 2020 A Battery Performance Analysis for Working Vehicle Applications in *IEEE Transactions on Industry Applications* **56**(1) pp 644-653
[6] Mocera F, Somà A and Clerici D 2020 Study of aging mechanisms in lithium-ion batteries for working vehicle applications *Fifteenth international conference on ecological vehicles and renewable energies (EVER)* (Monte-Carlo, Monaco)
[7] Vergori E, Mocera F and Somà A 2018 Battery Modelling and Simulation Using Programmable Testing Equipment *Computers* **7**(2) p 20
[8] Duane C Hanselman 2006 *Brushless Permanent Magnet Motor Design* Magna Physics Publishing
[9] Urresty J, Riba J, Romeral L and Garcia A 2010 A simple 2-D finite-element geometry for analyzing surface-mounted synchronous machines with skewed rotor magnets *IEEE Transactions on Magnetics* **46** pp 3948-54
[10] Mocera F and Somà A 2018 Working Cycle requirements for an electrified architecture of a vertical feed mixer vehicle *Procedia Structural Integrity*, **12** pp 213-223
[11] Lu D, Ouyang M, Gu J and Li J 2014 Instantaneous optimal regenerative braking control for a permanent-magnet synchronous motor in a four-wheel-drive electric vehicle *Proceedings of the Institution of Mechanical Engineers, Part D: Journal of Automobile Engineering* **228**(8) pp 894-908
[12] Berardi G and Bianchi N 2017 Rotor losses reduction in high speed PM generators for organic rankine cycle systems *IEEE Energy Conversion Congress and Exposition (ECCE)* **55**(6) pp 5800-08
[13] Huang J, Shervin S , Miller R, Rizzo D, Sebeck K, Shurin S, Wagner J et Al. 2019 A Hybrid Electric Vehicle Motor Cooling System- Design, Model, and Control *IEEE Transactions on Vehicular Technology* **68**(5) pp 4467-78
[14] Fan J, Zhang C, Wang Z, Dong Y, Nino C E, Rehman A and Strangas E 2010 Thermal Analysis

of Permanent Magnet Motor for the Electric Vehicle Application Considering Driving Duty Cycle. Magnetics*, IEEE Transactions* **46** pp 2493 – 96
[15] Sjökvist S 2014 Demagnetization Studies on Permanent Magnets *Uppsala Universitet*
[16] Egorov D, Petrov I, Pyrhönen J, Link J and Stern R 2017 Linear recoil curve demagnetization models for ferrite magnets in rotating machinery 43rd Annual Conference of the IEEE Industrial Electronics Society pp 2046-2052
[17] Zhilichev Y 2008 Analysis of Permanent Magnet Demagnetization Accounting for Minor B-H Curves *IEEE Transactions on Magnetics* **44**(11) pp 4285-88